# Effect of Transitional Layer on Frequency of Kink Oscillations

M.S. Ruderman[1,2,3] · N.S. Petrukhin[4]

**Abstract**
In this article we study the effect of a transitional layer in a magnetic tube on the real part of the frequencies of kink oscillations. In our analysis, we use the model of a straight magnetic tube with the density and cross-section radius varying along the loop, and the thin-tube thin-boundary (TTTB) approximation. First, we calculate the correction to the fundamental frequency and show that it is positive and of the order of the ratio of the transitional layer thickness to the loop radius $\ell$. The increase in the fundamental frequency results in the decrease in the estimate of the magnetic-field magnitude. Then we study the effect of the transitional layer on the ratio between the fundamental frequency and the first overtone frequency that is used for estimating the atmospheric scale height. We show that the correction to the frequency ratio is of the order of $\ell^2$, and thus it can be neglected for moderate values of $\ell$.

**Keywords** Sun · Plasma · Magnetohydrodynamics · Waves · Oscillations

## 1. Introduction

Transverse oscillations of coronal magnetic loops were first observed by the *Transition Region and Coronal Explorer* (TRACE) mission in 1998. The results of these observations were reported by Aschwanden et al. (1999) and Nakariakov et al. (1999). They were interpreted as kink oscillations of the magnetic-flux tubes. After that, the transverse oscillations of coronal magnetic loops were continuously observed by space missions (e.g., Erdélyi and Taroyan, 2008; Duckenfield et al., 2018; Su et al., 2018; Abedini, 2018, and references

✉ M.S. Ruderman
   m.s.ruderman@sheffield.ac.uk

1   Solar Physics and Space Plasma Research Centre (SP²RC), School of Mathematics and Statistics, University of Sheffield, Hicks Building, Hounsfield Road, Sheffield, S3 7RH, UK

2   Space Research Institute (IKI) Russian Academy of Sciences, Moscow, Russia

3   Moscow Center for Fundamental and Applied Mathematics, Lomonosov Moscow State University, Moscow, Russia

4   Higher School of Economics, National Research University, Moscow, Russia

therein). Kink oscillations were also observed in prominence threads (e.g., Arregui, Oliver, and Ballester, 2018). These oscillations are characterised by large amplitudes and quick damping.

The simplest model of a coronal magnetic loop is a straight magnetic tube with constant density inside and outside the tube and with immovable ends. Kink oscillations of such a tube were first studied in the thin-tube (TT) approximation, that is under the assumption that the tube radius is much smaller than the tube length, by Ryutov and Ryutova (1976) (see also Edwin and Roberts, 1983; Roberts, 2019). Later more advanced models of coronal magnetic loops were developed (see, e.g., the reviews by Ruderman and Erdélyi, 2009; Nakariakov et al., 2021). In particular, a straight magnetic tube with a transitional layer where the plasma density decreases from its value inside the tube to that of the plasma surrounding the tube was considered. The existence of the transitional-layer results in damping of kink waves caused by resonant absorption. Ruderman and Roberts (2002) calculated the decrement of kink oscillations of a magnetic tube with a transitional layer at its boundary. Using this result, they showed that the observed oscillation amplitude and the damping time can be used in coronal seismology to estimate the ratio of the thickness of the transitional layer to the tube radius [$\ell$] and thus obtain information on the internal structure of coronal loops. Goossens, Andries, and Aschwanden (2002) used this approach to estimate the ratio of the thickness of the transitional layer to the tube radius for eleven coronal magnetic loops. Dymova and Ruderman (2006) extended the analysis by Ruderman and Roberts (2002) to take the density variation along the magnetic loop into account, while Shukhobodskiy and Ruderman (2018) also included the cross-section radius variation along the loop. All analytical studies were carried out in the thin-tube and thin-boundary (TTTB) approximation. To go beyond this approximation, the numerical solution of the linearised magnetohydrodynamic (MHD) equations was used. The numerical study carried out by Van Doorsselaere et al. (2004a) showed that the TB approximation provide a fairly good approximation for the ratio of the transitional-layer thickness to the tube radius up to 0.5, that is in cases when the transitional layer does not look really thin. For a review of resonant damping of coronal-loop kink oscillations, see Goossens, Andries, and Arregui (2006) and Goossens, Erdélyi, and Ruderman (2011).

The presence of the transitional layer not only causes resonant absorption but also affects the oscillation frequency. Van Doorsselaere et al. (2004a) numerically calculated the complex eigenfrequency of kink oscillations of one-dimensional magnetic tube with the transitional layer. Although the article by Van Doorsselaere et al. (2004a) mainly deals with the damping due to resonant absorption, it was also obtained that the presence of transitional layer causes the increases of oscillation frequency. Later, the effect of the transitional layer on the oscillation frequency and its application to coronal seismology was studied by Soler et al. (2014) and Pascoe, Hood, and Van Doorsselaere (2019). In particular, they also found that the presence of the transitional layer increases the oscillation frequency. Hence, accounting for the transitional-layer presence can affect the seismological estimate of the magnetic-field magnitude in coronal loops. Usually, the kink oscillations of coronal loops are studied in the cold-plasma approximation. However, the same result is valid for a finite plasma-$\beta$ that is appropriate for using in applications to photosphere. Hence, the oscillation frequency increase due to the presence of transitional layer is a general property of kink oscillations.

The observations of coronal-loop kink oscillations are used in coronal seismology not only to obtain the information on the loop transverse structure and to estimate the magnetic-field magnitude, but also to estimate the atmospheric scale height in the corona. The latter estimate is based on the observation of the frequencies of the fundamental mode and the

first overtone of the coronal-loop kink oscillations. To our knowledge, the effect of the transitional layer on this estimate has not been discussed yet. To do so is the main aim of this article.

The article is organised as follows: In the next section we formulate the problem. In Section 3 we present the expression for the correction of the kink-oscillation frequency caused by the presence of the transitional layer. In Section 4 we study the effect of the transitional layer on the estimate of the magnetic-field magnitude. In Section 5 the effect of the transitional layer on the ratio of the periods of the fundamental mode and the first overtone is analysed. Section 6 contains the summary of the results and our conclusions.

## 2. Problem Formulation

We consider plasma motion using the zero-$\beta$ approximation. The equilibrium state is the same as in the article by Shukhobodskiy and Ruderman (2018: Article I). We model a coronal loop as a straight, thin, and expanding magnetic tube with a circular cross-section. The tube consists of a core and a transitional region where the density monotonically decreases from a higher value inside the tube to a lower value representing the surrounding plasma. In cylindrical coordinates $r, \phi, z$ with the $z$-axis coinciding with the tube axis, the equilibrium density is given by

$$\rho(r, z) = \begin{cases} \rho_i(r, z), & r \leq R(z)(1 - \ell/2), \\ \rho_t(r, z), & R(z)(1 - \ell/2) \leq r \leq R(z)(1 + \ell/2), \\ \rho_e(r, z), & r \geq R(z)(1 + \ell/2), \end{cases} \tag{1}$$

where $R(z)$ is the tube radius, $\ell$ is a constant, $\rho_e(r, z) < \rho_i(r, z)$, $\rho_t(r, z)$ is a monotonically decreasing function of $r$, $\rho(r, z)$ is continuous at $r = R(z)(1 \pm \ell/2)$, and $\ell R(z)$ is the thickness of the transitional layer. The domain defined by $r \leq R(z)(1 - \ell/2)$ is the core part of the magnetic tube, while $R(z)(1 - \ell/2) \leq r \leq R(z)(1 + \ell/2)$ is the transitional region. Below the subscripts "i" and "e" indicate that a quantity is calculated in the core part of the magnetic tube and in the external plasma, respectively. The equilibrium magnetic field is $\boldsymbol{B} = (B_r(r, z), 0, B_z(r, z))$. We assume that the boundaries of the transitional layer are magnetic surfaces. A sketch of the equilibrium is shown in Figure 1. We use the TTTB approximation and assume that $R(z) \ll L$ and $\ell \ll 1$, where $L$ is the loop length. We also assume that the characteristic scale of variation of $\rho_i$, $\rho_e$, and $\boldsymbol{B}$ in the radial direction is $L$. On the other hand, the characteristic scale of variation of $\rho_t$ in the radial direction is $\ell R_*$, where $R_*$ is a typical value of $R(z)$. Below we use the notation $R_*/L = \epsilon$. The tube ends are assumed to be frozen in the dense plasma at $z = \pm L/2$. It follows from Equation 1 that the ratio of the transitional-layer thickness to the tube radius is independent of $z$. In the thin tube approximation $B$ and $R$ are related by

$$B R^2 = \text{const.} \tag{2}$$

Plasma motion is described everywhere by the linearised ideal MHD equations, except in the vicinity of a resonant surface, where the oscillation frequency coincides with the local Alfvén frequency. In this vicinity, the viscosity is taken into account in order to remove a singularity in the ideal MHD equations.

**Figure 1** Sketch of the
equilibrium state.
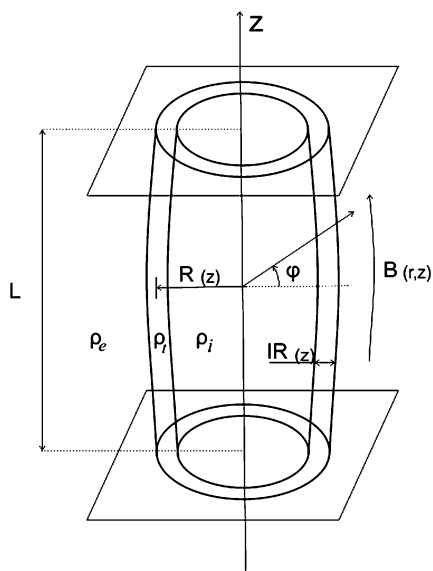


## 3. Expression for Oscillation Frequency

The frequency of magnetic-tube kink oscillation with the account of the transitional-layer
effect was calculated in Article I. In this article the following scaled variables were intro-
duced:

$$\Omega = \epsilon^{-1}\omega, \quad Z = \epsilon z, \tag{3}$$

where $\omega$ is the oscillation frequency. The plasma displacement perpendicular to $\boldsymbol{B}$ and in
the planes $\phi = $ const. is $\xi_\perp$. Below we use the variable $\eta = \xi_\perp / R(z)$, where $\xi_\perp$ is calculated
on the tube axis. The solution in Article I is given in the form of expansions

$$\eta = \eta_0 + \ell\eta_1 + \cdots, \quad \Omega = \Omega_0 + \ell\Omega_1 + \cdots \tag{4}$$

The solution in Article I is obtained in the form of Fourier expansions with respect to eigen-
functions of the following boundary-value problem:

$$V_A^2 \frac{\partial^2 Y}{\partial Z^2} = -\lambda Y, \quad Y(\pm R_*/2) = 0, \tag{5}$$

where $V_A^2 = B^2(\mu_0\rho)^{-1}$ is the Alfvén speed and $\mu_0$ is the magnetic permeability of free
space. The eigenvalues of this problem constitute a monotonically increasing sequence $\{\lambda_n\}$,
$\lambda_n \to \infty$ as $n \to \infty$ (Coddington and Levinson, 1955). The eigenfunctions of the boundary-
value problem satisfy the orthogonality condition

$$\int_{-R_*/2}^{R_*/2} V_A^{-2} Y_n Y_m \, dZ = 0, \quad \text{for } m \neq n, \tag{6}$$

and they are normalised by the condition

$$\int_{-R_*/2}^{R_*/2} V_A^{-2} Y_n^2 \, dZ = 1. \tag{7}$$

In particular, the following expansion was used (Equation 40 in Article I):

$$\Phi = \sum_{n=1}^{\infty} \Phi_n Y_n(Z), \tag{8}$$

where

$$\Phi = \frac{V_{\text{Ai}}^2 Q_{\text{i}}}{R^2}, \quad Q = \epsilon^{-2} \frac{P}{B^2}, \tag{9}$$

and $P$ is the perturbation of the magnetic pressure. The coefficient $\Phi_n$ in Equation 8 is given by (Equation 39 in Article I)

$$\Phi_n = \int_{-R_*/2}^{R_*/2} V_{\text{A}}^{-2} \Phi Y_n \, \mathrm{d}Z. \tag{10}$$

In Article I the flux function $\psi$ is defined by

$$B_r = -\frac{1}{r} \frac{\partial \psi}{\partial z}, \quad B_z = \frac{1}{r} \frac{\partial \psi}{\partial r}. \tag{11}$$

The function $\psi$ is used as an independent variable instead of $r$. In the thin-tube approximation, the relation between $\psi$ and $r$ is given by

$$\psi = \frac{1}{2} r^2 B. \tag{12}$$

It was assumed in Article I that the density in the transitional layer can be factorised and written as the product of two functions: one depending on $Z$, and the other depending on $\psi$. As a result, we obtain (Equation 35 in Article I)

$$V_{\text{A}}^2(\psi, Z) = V_{\text{Ai}}^2(Z) g(\psi), \quad g(\psi_{\text{i}}) = 1, \quad g(\psi_{\text{e}}) = \frac{V_{\text{Ae}}^2}{V_{\text{Ai}}^2}, \tag{13}$$

where $\psi = \psi_{\text{i}}$ and $\psi = \psi_{\text{e}}$ are the equations of the internal and external boundaries of the transitional layer, and

$$\psi_{\text{i}} = \frac{1}{2} B R^2 (1 - \ell/2)^2, \quad \psi_{\text{e}} = \frac{1}{2} B R^2 (1 + \ell/2)^2. \tag{14}$$

We note that the eigenvalues $[\lambda_n]$ and eigenfunctions $[Y_n]$ of the boundary value problem in Equation 5 depend on $\psi$.

The eigenfrequency $\Omega_0$ and the corresponding eigenfunction $\eta_0$ are defined by

$$C_{\text{k}}^2 \frac{\mathrm{d}^2 \eta_0}{\mathrm{d}Z^2} + \Omega_0^2 \eta_0 = 0, \quad C_{\text{k}}^2 = \frac{2B^2}{\mu_0 (\rho_{\text{i}} + \rho_{\text{e}})}, \quad \eta_0 = 0 \text{ at } Z = \pm R_*/2. \tag{15}$$

In Article I the equation determining $\Omega_1$ is obtained (Equation 71). It reads

$$\Omega_0 \Omega_1 \int_{-R_*/2}^{R_*/2} \frac{\eta_0^2}{C_{\text{k}}^2} \, \mathrm{d}Z = -\frac{1}{\ell} \int_{-R_*/2}^{R_*/2} \frac{\eta_0 \mathcal{L}_1[\eta_0]}{2C_{\text{k}}^2} \, \mathrm{d}Z - \mathrm{i}\Upsilon, \tag{16}$$

where (Equation 67 in Article I)

$$\mathcal{L}_1[\eta] = \frac{\mu_0 \rho_e}{B R^2 (\rho_i + \rho_e)} \mathcal{P} \int_{\psi_i}^{\psi_e} g(\psi) \sum_{n=1}^{\infty} \frac{[\Omega_0^2 - \lambda_n(\psi_e)] \Phi_n Y_n(Z)}{\Omega_0^2 - \lambda_n(\psi)} d\psi$$

$$+ \frac{2\ell B^2 Q_i}{R^2 (\rho_i + \rho_e)} + \frac{\Omega_0^2 \eta}{\rho_i + \rho_e} \left( \frac{1}{B R^2} \int_{\psi_i}^{\psi_e} \rho \, d\psi - \ell(3\rho_i - \rho_e) \right), \qquad (17)$$

$\Upsilon$ is a real quantity, and $\mathcal{P}$ indicates the principal Cauchy part of the integral. We do not give the expression for $\Upsilon$ because it will not be used below. It follows from Equation 16 that

$$\Re(\Omega_1) \int_{-R_*/2}^{R_*/2} \frac{\eta_0^2}{C_k^2} dZ = -\frac{1}{\ell \Omega_0} \int_{-R_*/2}^{R_*/2} \frac{\eta_0 \mathcal{L}_1[\eta_0]}{2 C_k^2} dZ, \qquad (18)$$

where $\Re$ indicates the real part of a quantity. Finally, the quantity $Q_i$ is defined by (Equation 75 in Article I)

$$Q_i = \frac{\rho_i \psi_i}{B^3} [\Omega_0^2 - \lambda_N(\psi_i)] \eta_0, \qquad (19)$$

and $N$ is determined by the condition that there is a value $\psi$ such that $\lambda_N(\psi) = \Omega_0^2$. It was assumed in Article I that the intervals $[\lambda_n(\psi_i), \lambda_n(\psi_e)]$, $n = 1, 2, \ldots$, do not intersect. This condition guarantees that $N$ is defined uniquely. However, in fact the analysis in Article I remains valid if we impose a weaker restriction that there is only one value of $N$ such that

$$\Omega_0^2 \in (\lambda_N(\psi_i), \lambda_N(\psi_e)). \qquad (20)$$

## 4. Effect of Transitional Layer on Magnetic-Field Estimate

Using observations of the transverse oscillations of the coronal magnetic loops is one of the most popular methods of coronal seismology. The first application of these observations for estimating the magnetic-field magnitude in coronal loops was made by Nakariakov and Ofman (2001). Following this article, we consider a magnetic tube homogeneous in the axial direction. The only difference is that Nakariakov and Ofman (2001) considered a magnetic tube with a sharp boundary, while we consider a tube with a transitional layer. Since now $B$, $\rho_i$, and $\rho_e$ are constants, it follows from Equation 15 that for the fundamental mode

$$\Omega_0 = \frac{\pi C_k}{R_*}, \quad \eta_0 = \cos \frac{\pi Z}{R_*}. \qquad (21)$$

Since $V_A$ is independent of $Z$ it follows from Equations 5 and 7 that

$$\lambda_{2n-1} = \frac{\pi^2 (2n-1)^2 V_A^2}{R_*^2}, \quad Y_{2n-1} = V_A \sqrt{\frac{2}{R_*}} \cos \frac{\pi (2n-1) Z}{R_*},$$

$$\lambda_{2n} = \frac{4\pi^2 n^2 V_A^2}{R_*^2}, \quad Y_{2n} = V_A \sqrt{\frac{2}{R_*}} \sin \frac{2\pi n Z}{R_*}, \qquad (22)$$

where $n = 1, 2, \ldots$ The condition $\lambda_1(\psi) = \Omega_0^2$ reduces to

$$2\rho_t(r) = \rho_i + \rho_e. \qquad (23)$$

Since $\rho_e \leq \rho_t(r) \leq \rho_i$ and $\rho_t(r)$ is a monotonically decreasing function, it follows that there is exactly one value $r = r_A$ for which Equation 23 is satisfied. On the other hand, the condition $\Omega_0^2 < \lambda_2(\psi_i)$ reduces to an obvious inequality $2(\rho_i + \rho_e) > \rho_i$. Hence, Equation 20 is satisfied only for $N = 1$.

Using Equations 14, 15, 19, and 21 we obtain

$$Q_i = \frac{\pi^2(\rho_i - \rho_e)}{2\mu_0(\rho_i + \rho_e)} \cos\frac{\pi Z}{R_*} + \mathcal{O}(\ell). \tag{24}$$

It follows from this result and Equations 10 and 22 that

$$\Phi_1 = \frac{\pi^2 V_{Ai}^2(\rho_i - \rho_e)\sqrt{2R_*}}{4\mu_0 R^2 V_A(\rho_i + \rho_e)}, \quad \Phi_n = 0, \ n = 2, 3, \ldots \tag{25}$$

To calculate $\mathcal{L}_1[\eta_0]$ we need to specify the function $\rho_t(r)$. Two popular forms of this function are linear and sinusoidal. Below we consider a more general density profile defined by

$$\rho_t(r) = \frac{\rho_i + \rho_e}{2} - \frac{\rho_i - \rho_e}{2}\chi(r), \tag{26}$$

where $\chi(r)$ is a monotonically increasing odd function of $r - R$ for $r \in [R(1 - \ell/2), R(1 + \ell/2)]$ satisfying the conditions $\chi(R(1 - \ell/2)) = -1$ and $\chi(R(1 + \ell/2)) = 1$. Now, it follows from Equation 23 that $r_A = R$. Using Equations 12, 13, 14, 22, and 25 we obtain

$$\mathcal{P}\int_{\psi_i}^{\psi_e} g(\psi) \sum_{n=1}^{\infty} \frac{[\Omega_0^2 - \lambda_n(\psi_e)]\Phi_n Y_n(Z)}{\Omega_0^2 - \lambda_n(\psi)} d\psi = 0. \tag{27}$$

This result follows from the fact that $\rho_t(C_k^2 - V_A^2)$ is an odd function of $r - R$. With the aid of this result and Equations 14, 21, 24, 26, and 27 we obtain from Equation 17 in the leading-order approximation with respect to $\ell$

$$\mathcal{L}_1[\eta_0] = -\frac{\ell(2\rho_i - \rho_e)}{\rho_i + \rho_e} \Omega_0^2 \cos\frac{\pi Z}{R_*}. \tag{28}$$

We emphasise that this equation is valid for the general density profile defined by Equation 26 with the function $\chi$ satisfying the conditions formulated after that equation. In particular, it is valid both for the linear as well as sinusoidal density profile. Substituting Equation 28 in Equation 18 and using Equation 21 yields

$$\Re(\Omega_1) = \frac{\Omega_0(2\rho_i - \rho_e)}{2(\rho_i + \rho_e)}. \tag{29}$$

Hence, the oscillation frequency calculated with an accuracy of up to terms of the order of $\ell$ is

$$\Omega = \Omega_0\left(1 + \frac{\ell(2\rho_i - \rho_e)}{2(\rho_i + \rho_e)}\right). \tag{30}$$

We see that the presence of a transitional layer increases the fundamental oscillation frequency. A similar result was previously obtained by Van Doorsselaere et al. (2004a), Goossens, Andries, and Arregui (2006), and Pascoe, Hood, and Van Doorsselaere (2019).

We also see that the second term in the brackets is smaller than $\ell/2$. When there is no transitional layer, the magnetic field is given by

$$B = \frac{\omega_0 L}{\pi} \sqrt{\frac{\mu_0(\rho_i + \rho_e)}{2}}, \tag{31}$$

where $\omega_0 = \epsilon \Omega_0$ is the non-scaled frequency of the fundamental mode of the kink oscillation, calculated without taking into account the transitional-layer effect. Using Equation 30, we rewrite this equation as

$$B \approx \frac{\omega L}{\pi} \sqrt{\frac{\mu_0(\rho_i + \rho_e)}{2}} \left(1 - \frac{\ell(2\rho_i - \rho_e)}{2(\rho_i + \rho_e)}\right). \tag{32}$$

Hence, if we take the effect of the transitional layer into account, then the estimate for the magnetic field must be reduced. Goossens, Andries, and Aschwanden (2002) used the observed damping rate of kink oscillations to estimate the thickness of transitional layer for 11 coronal magnetic loops. The maximum value they found was $\ell = 0.49$. This implies that the second term in brackets in Equation 32 is less than 1/2, but it can be close to this value. Therefore, accounting for the transitional-layer effect can reduce the estimate of the magnetic-field magnitude by almost 50%.

Nakariakov and Ofman (2001) were the first who used the observed kink oscillations of coronal loops to estimate the magnetic-field magnitude in coronal loops. They used the event observed by TRACE on 14 July 1998 and obtained that the magnetic-field magnitude is between 4 G and 30 G. Using the observed damping of the loop oscillations, Ruderman and Roberts (2002) found $\ell = 0.23$. Both Nakariakov and Ofman (2001) and Ruderman and Roberts (2002) took $\rho_i/\rho_e = 10$. Hence, accounting for transitional-layer effect reduces the estimate obtained by Nakariakov and Ofman (2001) by 17%. Therefore, the new boundaries for the magnetic-field magnitude are 3.3 G and 25 G. We can see that the reduction in the estimate of the magnetic-field magnitude introduced by the account of the transitional-layer effect is small in comparison with the uncertainty introduced by other factors.

## 5. Effect of Transitional Layer on Estimate of Atmospheric Scale Height

Verwichte et al. (2004) reported for the first time the simultaneous observations of the fundamental harmonic and the first overtone of the transverse oscillation of the coronal magnetic loops. A very important result was that the first overtone was less than twice the frequency of the fundamental mode. Andries, Arregui, and Goossens (2005) suggested that this effect is related to the density variation along the loop, and they developed a method of estimation of the atmospheric scale height in the corona using the ratio of frequencies of the first overtone and the fundamental mode of coronal-loop transverse oscillations. Ruderman, Verth, and Erdélyi (2008), Verth and Erdélyi (2008), and Verth, Erdélyi, and Jess (2008) extended the analysis by Andries, Arregui, and Goossens (2005) to take the loop expansion into account. For a review of the method of the atmospheric-scale-height estimation using the ratio of the frequencies of the first overtone and the fundamental mode of coronal-loop transverse oscillations, see Andries et al. (2009). In all these articles, a model of the magnetic tube with a sharp boundary was used. In this section we study the effects of transitional layer on the estimate of the atmospheric scale height.

We assume that a coronal magnetic loop is in a vertical plane, has a half-circular shape, and is immersed in an isothermal atmosphere. We also assume that the plasma temperature

is the same inside and outside the loop. Van Doorsselaere et al. ([2004b](#)) showed that the effect of curvature on the frequencies of coronal-loop transverse oscillations is of the order of $\epsilon$. Since for a typical coronal loop $\epsilon$ is of the order of 0.02, we can safely neglect the effect of curvature on the oscillation frequencies. Hence, the loop shape only affects the density variation along the loop caused by gravity. Since the temperature is the same inside and outside the loop, we obtain

$$\rho_e(z) = \frac{\rho_i(z)}{\zeta}, \quad \zeta = \text{const.} \tag{33}$$

The assumption that the characteristic scale of variation of $\rho_i$ and $\rho_e$ in the radial direction is $L$ enables us to neglect the radial dependence of these quantities and assume that they only depend on $z$. The density in the transitional layer $[\rho_t(r, z)]$ is given by Equation [26](#). Below we use the notation $\Omega_f$ and $\eta_f$ for the frequency and eigenfunction of the fundamental mode, and $\Omega_h$ and $\eta_h$ for the frequency and eigenfunction of the first overtone. $\Omega_{f0}$ and $\eta_{f0}$ are defined by Equation [15](#) with the condition that it does not have nodes in the interval $(-R_*/2, R_*/2)$. The frequency and eigenfunction of the first overtone are defined by

$$C_k^2 \frac{d^2 \eta_{h0}}{dZ^2} + \Omega_{h0}^2 \eta_{h0} = 0, \quad \eta_{h0} = 0 \text{ at } Z = -R_*/2 \text{ and } Z = 0, \tag{34}$$

with the condition that it does not have nodes in the interval $(-R_*/2, 0)$.

Using Equation [13](#), we transform Equation [5](#) to

$$V_{Ai}^2 \frac{\partial^2 Y}{\partial Z^2} = -\frac{\lambda(\psi)}{g(\psi)} Y, \quad Y(\pm R_*/2) = 0. \tag{35}$$

It follows from this equation that

$$\lambda_n(\psi) = g(\psi)\lambda_n(\psi_i), \quad Y_n = Y_n(Z), \tag{36}$$

that is $Y_n$ is independent of $\psi$. It follows from this result and Equations [9](#), [10](#), [12](#), [14](#), and [19](#) that in the leading-order approximation with respect to $\ell$

$$\Phi_n = \frac{\Omega_0^2 - \lambda_N(\psi_i)}{2\mu_0} \int_{-R_*/2}^{R_*/2} V_A^{-2} \eta_0(Z) Y_n(Z) \, dZ. \tag{37}$$

Comparing the eigenvalue problems defined by Equations [15](#) and [35](#), and using Equation [33](#), we obtain that

$$\Omega_{f0}^2 = \frac{C_k^2 \lambda_1(\psi_i)}{V_{Ai}^2} = \frac{2\zeta \lambda_1(\psi_i)}{\zeta + 1}, \quad \Omega_{h0}^2 = \frac{C_k^2 \lambda_2(\psi_i)}{V_{Ai}^2} = \frac{2\zeta \lambda_2(\psi_i)}{\zeta + 1}. \tag{38}$$

Then, using Equations [12](#) and [26](#), we obtain that $\Omega_{f0}^2 = \lambda_1(\psi_A)$ and $\Omega_{h0}^2 = \lambda_2(\psi_A)$, where $\psi_A$ is defined by equation

$$g(\psi_A) = \frac{2\zeta}{\zeta + 1}. \tag{39}$$

Since $g(\psi)$ monotonically increases from 1 to $\zeta$ in the interval $[\psi_i, \psi_e]$ there is exactly one value $\psi_A$ defined by this equation. It follows from Equations [36](#) and [38](#) that $\Omega_{f0} \in (\lambda_1(\psi_i), \lambda_1(\psi_e))$ and $\Omega_{h0} \in (\lambda_2(\psi_i), \lambda_2(\psi_e))$. We assume that $\Omega_{f0} < \lambda_2(\psi_i)$ and $\lambda_1(\psi_e) <$

$\Omega_{h0} < \lambda_3(\psi_i)$. Then it follows that $N$ is uniquely defined, and $N = 1$ for the fundamental mode and $N = 2$ for the first overtone. Below we describe the conditions when $N$ is uniquely defined for a particular equilibrium.

Finally, it follows that $\eta_{f0}$ is proportional to $Y_1$ and $\eta_{h0}$ is proportional to $Y_2$. Since $\eta$ has the dimension of length and, in accordance with Equation 7, $Y$ has the dimension of velocity divided by the square root of the length, we can take

$$\eta_{f0}(Z) = AY_1(Z), \quad \eta_{h0}(Z) = AY_2(Z), \tag{40}$$

where $A = V_*^{-1} R_*^{3/2}$ and $V_*$ is the characteristic value of the Alfvén speed.

First, we calculate $\Re(\Omega_{f1})$. Using Equations 6, 7, 37, 38, and 40 yields

$$\Phi_1 = \frac{A(\zeta - 1)}{4\mu_0 \zeta} \Omega_{f0}^2, \quad \Phi_n = 0, \ n = 2, 3, \ldots \tag{41}$$

With the aid of Equations 36, 38, 40, and 41, we obtain

$$\sum_{n=1}^{\infty} \frac{[\Omega_0^2 - \lambda_n(\psi_e)]\Phi_n Y_n(Z)}{\Omega_0^2 - \lambda_n(\psi)} = \frac{(\zeta - 1)^2 \Omega_{f0}^2 \eta_{f0}(Z)}{4\mu_0[(\zeta + 1)g(\psi) - 2\zeta]}. \tag{42}$$

Using this result and Equations 13, 17, and 38, we transform Equation 19 to

$$\mathcal{L}_1[\eta_{f0}] = \frac{W \Omega_{f0}^2 \eta_{f0}(Z)}{\zeta + 1}, \tag{43}$$

where

$$W = \frac{(\zeta - 1)^2}{4BR^2} \mathcal{P} \int_{\psi_i}^{\psi_e} \frac{g(\psi)\,d\psi}{(\zeta + 1)g(\psi) - 2\zeta} + \frac{\zeta}{BR^2} \int_{\psi_i}^{\psi_e} \frac{d\psi}{g(\psi)} - \frac{\ell(5\zeta - 1)}{2}. \tag{44}$$

It is straightforward to show that $W/\ell$ is independent of $\ell$, that is $W$ is a linear homogeneous function of $\ell$. Substituting this expression in Equation 16 and using Equation 43 yields

$$\Re(\Omega_{f1}) = -\frac{W \Omega_{f0}}{2\ell(\zeta + 1)}. \tag{45}$$

Repeating the same calculation, but for the first overtone, we obtain

$$\Re(\Omega_{h1}) = -\frac{W \Omega_{h0}}{2\ell(\zeta + 1)}. \tag{46}$$

Using Equations 45 and 46 yields

$$\frac{\Re(\Omega_h)}{\Re(\Omega_f)} = \frac{\Omega_{h0} + \ell\Re(\Omega_{h1})}{\Omega_{f0} + \ell\Re(\Omega_{f1})} + \mathcal{O}(\ell^2) = \frac{\Omega_{h0}}{\Omega_{f0}} + \mathcal{O}(\ell^2). \tag{47}$$

Hence, we see that the effect of the transitional layer on the ratio of the frequencies of the first overtone and the fundamental mode is weak, of the order of $\ell^2$ at best. Therefore, it can be safely neglected for $\ell \lesssim 0.3$. This conclusion is based on a few assumptions. One important assumption is that $N$ is uniquely defined both for the fundamental mode and the first overtone. This assumption is equivalent to two conditions:

$$\Omega_{f0}^2 < \lambda_2(\psi_i), \tag{48}$$
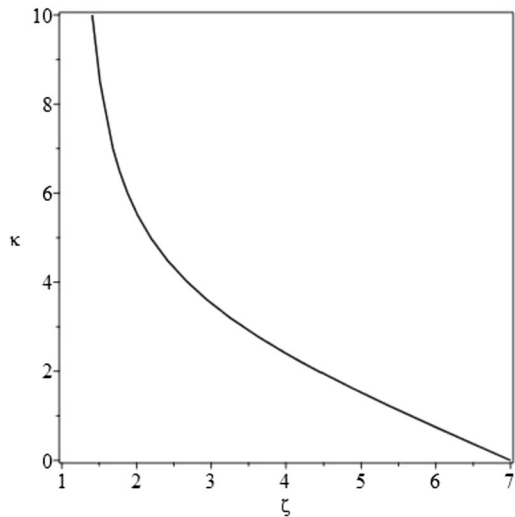
$$\lambda_1(\psi_e) < \Omega_{h0}^2 < \lambda_3(\psi_i). \tag{49}$$

Using Equation 38, it is straightforward to show that the inequality in Equation 48 follows
from the inequality in Equation 49. Then, again using Equation 38, we reduce the condition
given by Equations 48 and 49 to

$$\frac{\zeta+1}{2}\lambda_1(\psi_i) < \lambda_2(\psi_i) < \frac{\zeta+1}{2\zeta}\lambda_3(\psi_i). \tag{50}$$

As we have already pointed out, it is difficult to obtain conditions that must be imposed
on a loop of arbitrary shape and with arbitrary variation of the cross-section radius along
the loop to satisfy the conditions given by Equations 48 and 49. Hence, we only consider a
particular case of a coronal magnetic loop of a half-circular shape with the constant cross-
section radius. The density in this loop is given by

$$\rho_i(z) = \rho_0 \exp\left(-\frac{L}{\pi H}\cos\frac{\pi z}{L}\right), \tag{51}$$

where $\rho_0$ is the plasma density at the loop foot points, $H = k_B T/mg$ the atmospheric
scale height in the corona, $k_B \approx 1.38 \times 10^{-23}$ m$^2$ kg s$^{-2}$ K$^{-1}$ the Boltzmann constant,
$g = 274$ m s$^{-2}$ the gravity acceleration at the solar surface, and $m$ the mean mass per particle
(approximately equal to 0.6 times the proton mass). Equation 51 contains one free dimen-
sionless parameter $\kappa = L/\pi H$, which is the ratio of the loop height to the atmospheric scale
height. Hence, the eigenvalues $\lambda_n$ depend on $\kappa$ and we can write $\lambda_n(\psi; \kappa)$. The curve in
Figure 2 is defined by the equation

$$\lambda_2(\psi_i; \kappa) = \frac{\zeta+1}{2}\lambda_1(\psi_i; \kappa). \tag{52}$$

The left inequality in Equation 50 is satisfied for points $(\zeta, \kappa)$ that lie below the curve in
Figure 2. We verified numerically that the right inequality in Equation 50 is satisfied at least
for $\kappa \leq 10$. Hence, we conclude that the condition given by Equation 50 is satisfied for

points $(\zeta, \kappa)$ lying below the curve in Figure 2. In particular, if we take $\zeta = 3$ as a typical value for coronal magnetic loops, then Equation 50 is satisfied for $\kappa \lesssim 3$, that is even for the largest coronal loops.

## 6. Summary and Conclusion

In this article we studied the effect of a transitional layer on the frequency of kink oscillations of coronal magnetic-flux tubes. Traditionally, the main attention is paid to the imaginary part of this frequency that is responsible for the damping of the kink oscillations. However, in this article we studied the effects of transitional layer on the real part of the frequency. In our analysis, we used the results obtained by Shukhobodskiy and Ruderman (2018). These results were obtained using the model of a straight magnetic-flux tube with the density and radius of the tube cross-section varying along the tube, and the TTTB approximation.

First, we studied the effect of the transitional layer on the estimate of the magnetic-field magnitude. This estimate is based on the observed fundamental frequency of the kink oscillation. We showed that the presence of transitional layer increases the fundamental frequency. Previously, this result was obtained by Van Doorsselaere et al. (2004a), Goossens, Andries, and Arregui (2006), and Pascoe, Hood, and Van Doorsselaere (2019). The increase in the oscillation frequency leads to the decrease in the estimated magnetic-field magnitude. In particular, when the ratio of the transitional layer thickness and the tube radius [$\ell$] is equal to 0.5, the estimate of the magnetic-field magnitude is two times less than that obtained modelling coronal loops as magnetic tubes without a transitional layer.

The main aim of our analysis was to study the effect of the transitional layer on the ratio of frequencies of the fundamental mode and first overtone that is used to estimate the atmospheric scale height. The corrections for each of the two frequencies are of the order of $\ell$. However, we showed that the correction to the ratio of the frequencies is of the order of $\ell^2$ at best. Of course, when $\ell = 0.5$ this correction can be not very small, however for $\ell \lesssim 0.3$ it is less than or of the order of 10% and, thus, can be neglected.

## Declarations

## References

Abedini, A.: 2018, *Solar Phys.* **293**, 22. DOI.
Andries, J., Arregui, I., Goossens, M.: 2005, *Astrophys. J. Lett.* **624**, L57. DOI.
Andries, J., Van Doorsselaere, T., Roberts, B., Verth, G., Verwichte, E., Erdélyi, R.: 2009, *Space Sci. Rev.* **149**, 3. DOI.

Arregui, I., Oliver, R., Ballester, J.L.: 2018, *Liv. Rev. Solar Phys.* **15**, 3. DOI.
Aschwanden, M.J., Fletcher, L., Schrijver, C.J., Alexander, D.: 1999, *Astrophys. J.* **520**, 880. DOI.
Coddington, E.A., Levinson, N.: 1955, *Theory of Ordinary Differential Equations*, McGraw-Hill, New York.
Duckenfield, T., Anfinogentov, S.A., Pascoe, D.J., Nakariakov, V.M.: 2018, *Astrophys. J. Lett.* **854**, L5. DOI.
Dymova, M., Ruderman, M.S.: 2006, *Astron. Astrophys.* **457**, 1059. DOI.
Edwin, D.D., Roberts, B.: 1983, *Solar Phys.* **88**, 179.
Erdélyi, R., Taroyan, Y.: 2008, *Astron. Astrophys.* **489**, L49. DOI.
Goossens, M., Andries, J., Arregui, I.: 2006, *Phil. Trans. Roy. Soc. A* **364**, 433. DOI.
Goossens, M., Andries, J., Aschwanden, M.J.: 2002, *Astron. Astrophys.* **394**, L39. DOI.
Goossens, M., Erdélyi, R., Ruderman, M.S.: 2011, *Space Sci. Rev.* **158**, 289. DOI.
Nakariakov, V.M., Ofman, L.: 2001, *Astron. Astrophys.* **372**, L53. DOI.
Nakariakov, V.M., Ofman, L., DeLuca, E.E., Roberts, B., Davila, J.M.: 1999, *Science* **285**, 862. DOI.
Nakariakov, V.M., Anfinogentov, S.A., Antolin, P., Jain, R., Kolotkov, D.Y., Kupriyanova, E.G., Li, D., Magyar, N., Nisticò, G., Pascoe, D.J., Srivastava, A.K., Terradas, J., Vasheghani Farahani, S., Verth, G., Yuan, D., Zimovetz, I.V.: 2021, *Space Sci. Rev.* **217**, 73. DOI.
Pascoe, D.J., Hood, A.W., Van Doorsselaere, T.: 2019, *Front. Astron. Astrophys.* **6**, 22. DOI.
Roberts, B.: 2019, *MHD Waves in the Solar Atmosphere*, Cambridge University Press, Cambridge, UK.
Ruderman, M.S., Erdélyi, R.: 2009, *Space Sci. Rev.* **149**, 199. DOI.
Ruderman, M.S., Roberts, M.P.: 2002, *Astrophys. J.* **577**, 475. DOI.
Ruderman, M.S., Verth, G., Erdélyi, R.: 2008, *Astrophys. J.* **686**, 694. DOI.
Ryutov, D.D., Ryutova, M.P.: 1976, *Sov. Phys. JETP* **43**, 491.
Shukhobodskiy, A.A., Ruderman, M.S.: 2018, *Astron. Astrophys.* **615**, A156. DOI.
Soler, R., Goossens, M., Terradas, J., Oliver, R.: 2014, *Astrophys. J.* **781**, 111. DOI.
Su, W., Guo, Y., Erdélyi, R., Ning, Z.J., Ding, M.D., Cheng, X., Tan, B.L.: 2018, *Sci. Rep.* **8**, 4471. DOI.
Van Doorsselaere, T., Andries, J., Poedts, S., Goossens, M.: 2004a, *Astrophys. J.* **606**, 1223. DOI.
Van Doorsselaere, T., Debosscher, A., Andries, J., Poedts, S.: 2004b, *Astron. Astrophys.* **424**, 1065. DOI.
Verth, G., Erdélyi, R.: 2008, *Astron. Astrophys.* **486**, 1015. DOI.
Verth, G., Erdélyi, R., Jess, D.B.: 2008, *Astrophys. J.* **687**, L45. DOI.
Verwichte, E., Nakariakov, V.M., Ofman, L., DeLuca, E.E.: 2004, *Solar Phys.* **223**, 77. DOI.